Effective Hamiltonian for FeAs-based superconductors

Efstratios Manousakis,[1,2] Jun Ren,[3] Sheng Meng,[3] and Efthimios Kaxiras[3]

[1]*Department of Physics and MARTECH, Florida State University, Tallahassee, Florida 32306-4350, USA*

[2]*Department of Physics, University of Athens, Panepistimioupolis, Zografos, 157 84 Athens, Greece*

[3]*Department of Physics and School of Engineering and Applied Sciences, Harvard University, Cambridge, Massachusetts 02138, USA*
(Received 20 June 2008; published 19 November 2008)

The recently discovered FeAs-based superconductors show intriguing behavior and unusual dynamics of electrons and holes which occupy the Fe d orbitals and As $4s$ and $4p$ orbitals. Starting from the atomic limit, we carry out a strong-coupling expansion to derive an effective Hamiltonian that describes the electron and hole behaviors. The hopping and the hybridization parameters between the Fe d and As s and p orbitals are obtained by fitting the results of our density-functional-theory calculations to a tight-binding model with nearest-neighbor interactions and a minimal orbital basis. We find that the effective Hamiltonian, in the strong on-site Coulomb-repulsion limit, operates on three distinct subspaces coupled through Hund's rule. The three subspaces describe different components (or subsystems): (a) one spanned by the $d_{x^2-y^2}$ Fe orbital, (b) one spanned by the degenerate atomic Fe orbitals d_{xz} and d_{yz}, and (c) one spanned by the atomic Fe orbitals d_{xy} and d_{z^2}. Each of these Hamiltonians is an extended $t-t'-J-J'$ model and is characterized by different coupling constants and filling factors. For the case of the undoped material the second subspace alone prefers a ground state characterized by a spin-density-wave order similar to that observed in recent experimental studies, while the other two subspaces prefer an antiferromagnetic order. We argue that the observed spin-density-wave order minimizes the ground-state energy of the total Hamiltonian.

PACS number(s): 74.70.−b, 74.25.Ha, 74.25.Jb, 75.10.−b

I. INTRODUCTION

The recent observation of superconductivity in quaternary oxypnictides,[1–6] which are materials based on FeAs (and FeP), has rekindled intense activity[7–28] to find a description of the strong electronic correlations present in these materials and in the cuprates which could be responsible for such phenomena.

The structure of the new materials[2] (Fig. 1) consists of FeAs layers sandwiched between LaO layers with rather weak interlayer coupling. The FeAs layers consist of a square lattice formed by the Fe atoms, while the As atoms, which sit just above and just below the plane (see Fig. 1), form FeAs$_4$ octahedra squeezed along the c axis such that each Fe-As bond forms a $\pm 30°$ angle with the Fe plane.

As a function of temperature, the resistivity of the undoped parent compound, which is not an insulator, shows a drop around 150 K (Refs. 2 and 29) before turning back below 50 K. In addition, the magnetic susceptibility also shows an anomaly at 150 K and it was argued[29] that the parent material has a spin-density-wave (SDW) instability below 150 K. Recent neutron-diffraction studies[30] demonstrate that the parent compound at 150 K undergoes a structural distortion from tetragonal at high temperature to monoclinic at low temperature. Furthermore, these neutron-diffraction studies show that below ~134 K, while in the monoclinic phase, it develops the SDW order shown in Fig. 1. Subsequent Mössbauer and muon spin rotation (μSR) studies[31] confirmed these findings: the structural transition is found to be around 156 K and the magnetic transition around 138 K. The structural distortion which brings about the monoclinic structure at low temperature is such that the rows of atoms which have their spins antiferromagnetically aligned are closer than the rows of atoms in the perpendicular direction.

The electronic structure of LaO$_{1-x}$F$_x$FeAs has been studied by density-functional theory[7,11] (DFT) and by dynamical mean-field theory.[9] There are arguments against phonon-mediated superconductivity[9,10] in LaO$_{1-x}$F$_x$FeAs. In addition, there are suggestions that a two-band model[16–19,22] may be the right effective Hamiltonian to use in order to describe the low-energy physics of these materials.

Since the interlayer coupling is found to be weak,[11] in order to provide a simpler basis to understand the electronic structure of these materials we will focus on a single FeAs layer. As further justification of this choice, we have calculated the band structure of LaOFeAs and that of a single FeAs layer within density-functional theory and we find that the important features of the bands near the Fermi level ob-
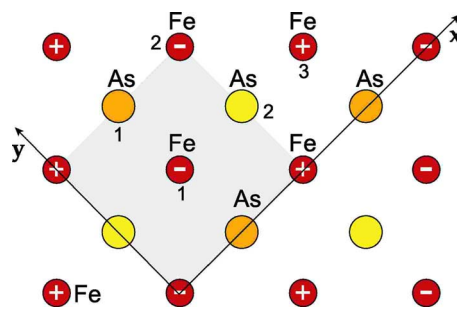

FIG. 1. (Color online) The structure of the FeAs layer in the FeAs-based superconductors. The Fe atoms form a square lattice while the As atoms form two square sublattices one just above (orange) and the other just below (yellow) the Fe plane. The **x** and **y** axes used to characterize the orbitals are shown and the unit cell is indicated by the shaded square. The + and − signs on the Fe atoms denote the spin orientation observed in the neutron-scattering experiment (Ref. 30). The labels are used in the text to explain the various types of antiferromagnetic exchange interactions.

tained by the two calculations are essentially the same, including position relative to the Fermi level and overall dispersion features. Accordingly, our starting point is a Hamiltonian which includes the five Fe d orbitals and four outer As orbitals ($4s$ and $4p$). In our interacting-electron model we include direct Fe-Fe hopping, hybridization between the Fe d and the As $4s$ and $4p$ orbitals, the local Coulomb-repulsion energy for adding an electron on any of the Fe d states via Hubbard-type terms in the Hamiltonian, and finally, coupling through Hund's rule.

We determine the relative energy of the atomic orbitals as well as the hopping and the hybridization matrix elements as follows: We carry out a set of first-principles calculations of the electronic structure of a single FeAs layer. Using as basis the above-mentioned Fe and As states, we fit the results of the first-principles calculations using the tight-binding (TB) approximation to determine the values of the hopping matrix elements and the on-site energy levels. We find that the energy difference between the atomic orbitals is less than 1 eV while the Coulomb repulsion to add two electrons on the same Fe d orbital is assumed to be significantly larger.[11–15,28] We perform a strong-coupling expansion in which the hopping and hybridization terms are used as perturbation and the unperturbed parts are the terms which correspond to the Coulomb-repulsion energies for a pair of electrons placed on the same or different orbitals. Even in the case where these classes of materials do not fulfill the requirement for a strong-coupling expansion, the qualitative results or trends suggested by such a systematic analysis may still be useful. We systematically derive a low-energy effective Hamiltonian to describe this multiband system.

Through this analysis, we show that the relevant low-energy degrees of freedom can be described by two "two-flavor" subsystems, one in which the two flavors correspond to electrons in the d_{xy} and d_{z^2} states of the Fe atoms and another in which the two flavors correspond to the d_{xz} and d_{yz} Fe orbitals, and a third one-flavor subsystem corresponding to the $d_{x^2-y^2}$ orbital. Each of those subsystems is described by a $t-t'-J-J'$ model where the spin degrees of freedom of all three subsystems couple through Hund's rule. Using this Hamiltonian we are able to explain why the undoped material orders in the SDW pattern shown in Fig. 1 as reported by recent neutron-scattering experiments.[30]

The paper is organized as follows. Section II gives a detailed discussion of our density-functional-theory band-structure calculations. Section III presents the strong-coupling limit analysis which leads to the effective spin-spin interaction Hamiltonian derived in Sec. IV. Section V gives a discussion of the physics of the effective Hamiltonian.

II. ELECTRONIC STRUCTURE CALCULATIONS

A. First-principles electronic structure

Our first-principles calculations are performed within the framework of DFT and the local-density approximation (LDA) for exchange-correlation effects. We used the SIESTA code[32] because it employs a localized basis of atomiclike orbitals for the expansion of the wave functions which makes the interpretation of electronic wave functions in the solid
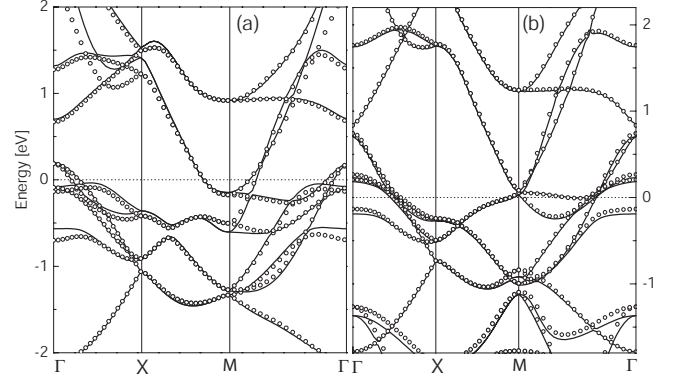

FIG. 2. The band structure obtained from the LDA calculations for the paramagnetic phase of (a) the LaOFeAs compound and (b) the FeAs layer. In both cases the lines are from the SIESTA calculations and the points from the VASP calculation. The Fermi level is set at zero in each case for the neutral material.

straightforward and transparent without the need for additional analysis such as projection to localized Wannier-type orbitals. We use pseudopotentials of the Troullier-Martins type[33] to represent the interaction between valence electrons and ionic cores, and the Ceperley-Alder form for the exchange-correlation functional.[34] We have generated several different Fe pseudopotentials in order to check for any dependence of the results on this ingredient of the calculations. We find that the effect of the different pseudopotentials on the quantities reported in the following, such as the electronic bands, is indiscernible. In addition to the SIESTA calculations, we have used the VASP code to ensure that there is reasonable agreement between the results of two very different computational schemes. The VASP code uses a plane-wave basis instead of localized orbitals[35] and employs pseudopotentials of a different type[36] than those in the SIESTA calculation.

LaOFeAs, belonging to the tetragonal $P4/nmm$ space group, has a layered structure.[2] The FeAs layer serves as the carrier conduction channel and it has strong electronic couplings within the layer. The unit cell for the simplified model system, a single FeAs layer, contains two Fe and two As atoms with a vacuum layer with a thickness of ~ 19 Å. The full system bulk LaOFeAs has two atoms of each type (Fe, As, La, and O) in the unit cell.

In the SIESTA calculations, we choose an auxiliary real-space grid equivalent to a plane-wave cutoff of 100 Ry and use an $8 \times 8 \times 1$ Monkhorst-Pack k-point grid for the FeAs layer, a $4 \times 4 \times 1$ grid for the (2×2) FeAs supercell, and a $8 \times 8 \times 4$ grid for the LaOFeAs structure. For geometry optimization, a structure is considered fully relaxed when the magnitude of forces on all atoms is smaller than 0.04 eV/Å. In the VASP calculation we use the same k-point grids and the default plane-wave cutoffs.

The results obtained for bulk LaOFeAs and for the FeAs layer, using the SIESTA and VASP codes, for the paramagnetic phase are shown in Fig. 2. In both cases, the agreement between the two different computational schemes is remarkable. Moreover, there is a very close similarity between the bands of the bulk LaOFeAs compound and the FeAs layer,
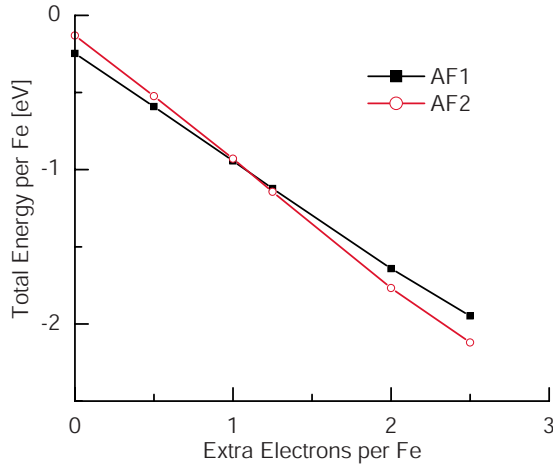
FIG. 3. (Color online) The total energy of the FeAs layer as a function of the added charge obtained with the VASP code. The reference energy is the energy of the neutral layer in the paramagnetic phase.

FIG. 4. The band structure of FeAs layer in the paramagnetic phase obtained from (a) the LDA calculations with the two different approaches (SIESTA—lines and VASP—points) and (b) the tight-binding approximation with nearest-neighbor interactions and minimal orbital basis.

especially in what concerns the features near the Fermi level. Notice that the neutral FeAs layer contains a different number of electrons per Fe atom than the bulk LaOFeAs compound. Accordingly, we show the Fermi levels for the bulk and the layer slightly offset to emphasize the similarity of the band-structure features. Moreover, by examining carefully the wave-function character of the bands near Γ and M, the points in the Brillouin zone where electron and hole pockets appear in the bulk LaOFeAs compound, we establish that these states arise from orbitals associated with the Fe and As atoms. For these reasons, it is reasonable to concentrate on the band structure of the FeAs layer alone in order to build a comprehensive picture of the interacting-electron system, presented in Secs. III and IV.

We address next the issue of the spin configuration. We considered different spin configurations in the antiferromagnetic (AFM) phase. For these calculations we use a (2×2) FeAs supercell. The two spin configurations are (i) AFM1, which is simply repetition of the spin configuration in the (1×1) unit cell and (ii) AFM2, which has the same spin alignment in one of the two diagonal directions of the Fe lattice and alternating spins along the other direction, as shown in Fig. 1. The total energy for the former spin configuration is lower by 0.95 eV per (2×2) cell, suggesting that the AFM1 configuration is more stable than the AFM2 one for the neutral FeAs layer. We believe that this result is due to the fact that our calculation is for the charge neutral FeAs layer, where the Fermi level is lower than that of the LaOFeAs compound; namely, the FeAs layer as part of the LaOFeAs structure is negatively charged by an extra electron per Fe atom because the LaO layer is positively charged since the preferred oxidation state of La is La^{3+} and that of oxygen is O^{2-}. To show that this is the case, we carried out a calculation using the VASP code for a charged FeAs layer. In Fig. 3 the total energies of the AFM1 and AFM2 phases are compared as a function of the added charge σ per Fe atom. Notice that the AFM2 phase becomes energetically favorable for $\sigma \sim 1$. The exact values of σ cannot be accurately determined in the context of these calculations because the energy
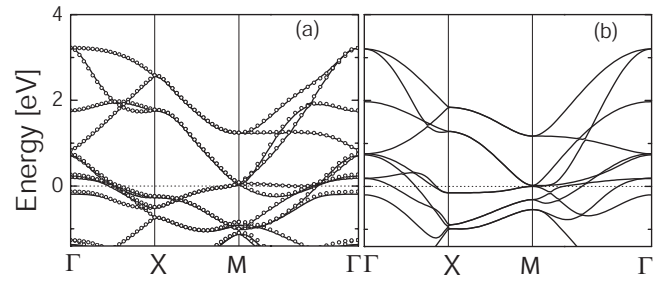
differences are within the range of accuracy of DFT-LDA. The fact that the AFM2 phase becomes the ground state for $\sigma = 1$ will be established using the effective Hamiltonian derived in Sec. II B, which captures the interacting-electron nature of the system in a more realistic manner, and as such gives more reliable results for the magnetic phases.

B. Tight-binding approximation model

Our goal next is to calculate a tight-binding Hamiltonian which approximately gives the same band structure as that of the first-principles results for the FeAs layer using nearest-neighbor (nn) interactions only (hopping matrix elements) and a minimal orbital basis, consisting of the $4s$ and $4p$ As orbitals and the $3d$ Fe orbitals. We expect that the hopping matrix elements, needed for the Hamiltonian upon which the strong-coupling expansion will be based, are not significantly affected by the value of the filling factor (the position of the Fermi level). For the reasons discussed above, namely, that a realistic picture of spin configurations can only arise from the interacting-electron treatment based on the effective Hamiltonian, we will focus on reproducing with the tight-binding approximation the band structure of the paramagnetic phase, as obtained from the DFT-LDA calculations.

Since the introduction of electron doping is necessary in order to produce superconductivity in LaOFeAs-based materials, we focus in reproducing as accurately as possible the features near and above the Fermi level. Note that hole-doping induced superconductivity in these materials has been also reported recently.[6] We also use information from the first-principles electronic wave functions to determine what is the optimal fit of the tight-binding approximation to the DFT-LDA results. As mentioned above, all the bands in the neighborhood of the Fermi level are associated with the As $4s$ and $4p$ and the Fe $3d$ orbitals, and these features are well reproduced by the tight-binding approximation results. The best fit we could achieve is shown in Fig. 4 and compared to the first-principles results for an extended region near the Fermi level. The on-site and hopping matrix elements that produce this fit are presented in Sec. III, where these values are employed to construct the effective Hamiltonian.

TABLE I. The on-site energies in eV for the Fe $3d$ orbitals as determined by approximating the results of the first-principles band-structure calculation using the tight-binding approximation discussed in Sec. II. We also include the hopping matrix elements $t_{\nu\nu}$ between two nearest-neighbor Fe d orbitals of the same type. The notation is explained in Sec. III.

ν	1	2	3	4	5
Fe $3d$ orbital	$d_{x^2-y^2}$	d_{xz}	d_{yz}	d_{xy}	d_{z^2}
$\epsilon_d(\nu)$	−4.6	−4.5	−4.5	−4.5	−4.2
$t_{\nu\nu}$	0.22	0.5	0.5	0.43	0.22

III. STRONG COUPLING LIMIT

We consider the Hamiltonian describing a single FeAs layer of Fe and As (or, in a more general formulation, P) atoms,

$$\hat{H} = \hat{H}_a + \hat{T} + \hat{U}, \tag{1}$$

with the three terms defined by

$$\hat{H}_a = \sum_{i,\nu,\sigma} \epsilon_d(\nu) d_{i\sigma}^{(\nu)\dagger} d_{i\sigma}^{(\nu)} + \sum_{l,\alpha,\sigma} \epsilon_{sp}(\alpha) sp_{l\sigma}^{(\alpha)\dagger} sp_{l\sigma}^{(\alpha)}, \tag{2}$$

$$\hat{T} = - \sum_{\langle ij\rangle,\sigma,\nu\nu'} (t_{\nu\nu'} d_{j\sigma}^{(\nu')\dagger} d_{i\sigma}^{(\nu)} + \text{H.c.})$$
$$- \sum_{i,\sigma,\nu,\alpha} \sum_{l(i)} (V_{il}^{\nu\alpha} d_{i\sigma}^{(\nu)\dagger} sp_{l\sigma}^{(\alpha)} + \text{H.c.}), \tag{3}$$

$$\hat{U} = \sum_{\nu} U_\nu^{(d)} \sum_i n_d^\nu(i\uparrow) n_d^\nu(i\downarrow) + \sum_{\nu,\nu'\neq\nu} U_{\nu\nu'}^{(d)} \sum_{i\sigma\sigma'} n_d^\nu(i\sigma) n_d^{\nu'}(i\sigma')$$
$$+ \sum_{\alpha} U_\alpha^{(sp)} \sum_i n_{sp}^\alpha(i\uparrow) n_{sp}^\alpha(i\downarrow)$$
$$+ \sum_{\alpha,\alpha'\neq\alpha} U_{\alpha\alpha'}^{(sp)} \sum_{i\sigma\sigma'} n_{sp}^\alpha(i\sigma) n_{sp}^{\alpha'}(i\sigma')$$
$$- \sum_{\nu,\nu'} J_{\nu,\nu'}^H \sum_i \vec{S}_d^\nu(i) \cdot \vec{S}_d^{\nu'}(i). \tag{4}$$

We discuss the noninteracting parts, $\hat{H}_a$ and $\hat{T}$, of the Hamiltonian first. The operator $d_{i\sigma}^{(\nu)\dagger}$ creates an electron of spin σ on the νth Fe d orbital ($\nu=1$, 2, 3, 4, and 5 are the indices that correspond to the five Fe d orbitals, $d_{x^2-y^2}$, d_{xz}, d_{yz}, d_{xy}, and d_{z^2}, respectively) at site i which has an energy $\epsilon_d(\nu)$. The operator $sp_{l\sigma}^{(\alpha)\dagger}$ creates an electron of spin σ on the αth As which is one of the *three* As orbitals. These As orbitals are formed as follows. First, because of the tetragonal symmetry, the two $4p_x$ and $4p_y$ orbitals remain unhybridized, while the $4s$ and $4p_z$ As states form two linear combinations $|sp_z^\pm\rangle = a|s\rangle \pm b|p_z\rangle$. The LDA calculation shows that the As sp_z^- state together with the Fe $4s$ state forms bonding and antibonding states where the bonding state is approximately 10 eV below the Fermi level and the antibonding state is approximately 6 eV above the Fermi level. Therefore, these two states are not included in the tight-binding fit and the three As states included are the $4p_x$ and $4p_y$ orbitals and the

TABLE II. Same as in Table I but for the As $4s4p$ orbitals.

α	1	2	3
As sp orbital	p_x	p_y	sp_z^+
$\epsilon_{sp}(\alpha)$	−4.7	−4.7	−5.2

sp_z^+ hybrid. Thus, $\alpha=1$, 2, and 3 corresponds to the cases of $4p_x$, $4p_y$, and sp_z^+, respectively, at the lth As site with site energy $\epsilon_{sp}(\alpha)$.

V is the hybridization term between the Fe $3d$ orbitals and the As orbitals. The sum over $l(i)$ means that it is over all four As sites l around the ith Fe site. The hybridization matrix element $V_{il}^{\nu\alpha}$ is proportional to the wave-function overlap of the νth Fe d orbital and the αth As sp orbital. Some of these matrix elements are zero due to symmetry arguments and the most significant ones are of the order of, or less than, 1 eV, as obtained through our tight-binding fit of the LDA results.

In Tables I–III we give the nonzero matrix elements obtained by fitting the LDA results to the tight-binding model (as explained in Sec. II) which includes the five Fe d states and the three As $4s$-$4p$ states for each of the two Fe and the two As atoms in the Fe_2As_2 unit cell, as well as the matrix elements $t_{\nu\nu'}$ and $V^{\nu\alpha}$ between these states. In addition to the above terms, the tight-binding approximation to the LDA results gives two hopping matrix elements $t_{\nu\nu'}$: the first for $\nu \to d_{xz}$ and $\nu' \to d_{yz}$, which is $t_{xz,yz}=0.54$ eV, and the second for $\nu \to d_{xy}$ and $\nu' \to d_{z^2}$, which is $t_{xy,z^2}=0.20$ eV. All other hopping matrix elements are either identically equal to zero due to symmetry or negligibly small.

We turn next to the interaction part, $\hat{U}$, of the Hamiltonian. $n_d^\nu(i\sigma) = d_{i\sigma}^{(\nu)\dagger} d_{i\sigma}^{(\nu)}$ is the number operator and $U_\nu^{(d)}$ or $U_\alpha^{(sp)}$ give the Coulomb repulsion for a pair of electrons placed on the same d orbital or the same s or p As orbital. $U_{\nu\nu'}^{(d)}$ (or $U_{\alpha\alpha'}^{(sp)}$) is responsible for the Coulomb repulsion between different Fe d (or As sp) orbitals within the same atom. We will assume that the Coulomb-repulsion terms between the same or different Fe d orbitals are significantly greater than their counterparts for the As sp states, consistent with the general expectations for these values in the literature: $U^{(d)}$ is believed to be large of the order of 4–5

TABLE III. Same as in Table I but for the hybridization matrix elements between Fe $3d$ and As $4s4p$ orbitals. The atom labels are those shown in Fig. 1. For the case of Fe atom labeled 2 in Fig. 1 the matrix elements are obtained from the same table by interchanging labels 1 and 2 of the As orbitals and reversing the sign.

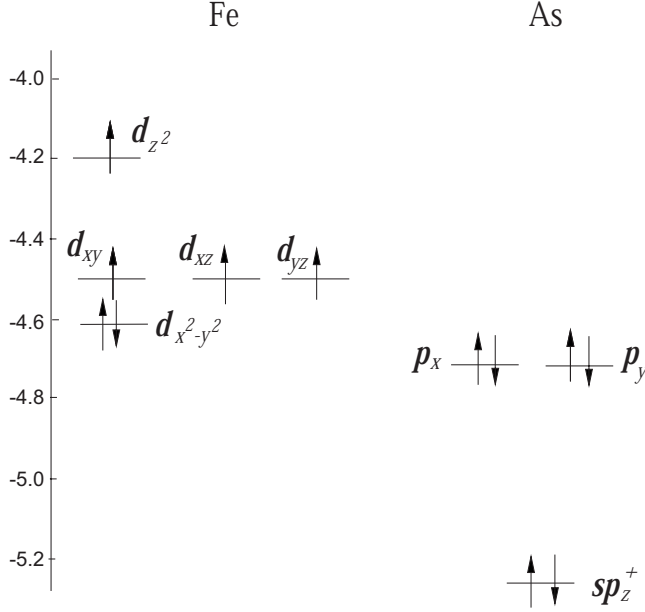| $V^{\nu\alpha}$	$1(d_{x^2-y^2})$	$2(d_{xz})$	$3(d_{yz})$	$4(d_{xy})$	$5(d_{z^2})$
$p_x(1)$	0	0.1	0	−0.2	0
$p_x(2)$	0.4	−1.45	0	0	0.25
$p_y(1)$	−0.4	0	1.45	0	0.25
$p_y(2)$	0	0	−0.1	−0.2	0
$sp_z^+(1)$	−0.5	0	0.7	0	0.9
$sp_z^+(2)$	−0.5	0.7	0	0	−0.9

FIG. 5. The occupation of the Fe and As atomic levels in the FeAs plane of the undoped parent compound. The ordering of the levels is shown schematically, as obtained from the tight-binding approximation parameters.

eV,[11–15,28] while the parameter $U^{(sp)}$ is expected to be much smaller than that. In addition, we will assume that the same site Fe d Coulomb repulsion is larger than the interorbital Coulomb repulsion $U^{(d)}_{\nu\nu'}$. The term proportional to J^H represents Hund's rule for the Fe d orbitals, with $J^H > 0$, of the order of less than 1 eV. We have neglected Hund's rule coupling for As orbitals.

Notice that the energy levels $\epsilon_d(\nu)$ and $\epsilon_{sp}(\nu)$ lie in the region of -4.7 ± 0.5 eV; namely, the energy difference between any pair of such states is less than 1 eV which is believed to be smaller than the characteristic Coulomb-repulsion energy $U^{(d)}$. In this paper we begin our analysis from the atomic or strong-coupling limit, which implies that we have assumed that the energy scale U^* defined below in Eq. (17) is significantly larger than the hopping and hybridization matrix elements. If this condition is not fulfilled for this class of materials, it may still be instructive to discuss the qualitative features which a strong-coupling expansion yields. In this limit the unperturbed part of the Hamiltonian $\hat{H}_0$ is

$$\hat{H}_0 = \hat{H}_a + \hat{U}, \tag{5}$$

and the hopping part $\hat{T}$, which includes the hybridization, plays the role of perturbation. As discussed previously, the FeAs layer in the undoped LaOFeAs parent compound has an additional electron relative to the neutral FeAs layer. This is due to the fact that LaO layer is expected to be in combined 1+ oxidation state. Therefore, the eight states considered above (five Fe d states plus three As sp states) are occupied by 12 electrons. The atomic configuration is shown in Fig. 5. Since we have five more electrons than levels, five energy levels must be doubly occupied. Double occupancy

of the Fe d orbitals is much more costly compared to the As sp orbitals; therefore, all three of the As orbitals must be doubly occupied and the only doubly occupied Fe d orbital is $d_{x^2-y^2}$, which has the lowest energy. The other four Fe d orbitals are singly occupied and the spins of these electrons are parallel because of Hund's rule, represented by the coupling J_H.

Next we consider the effective Hamiltonian which, in strong-coupling perturbation theory, is given by

$$\hat{H}_{\text{eff}} = E_0 \hat{P}_0 + \hat{P}_0 \hat{T} \hat{\Omega}, \tag{6}$$

$$\hat{\Omega} = \hat{P}_0 + \hat{R}(\hat{T}\hat{\Omega} - \hat{\Omega}\hat{T}\hat{\Omega}), \tag{7}$$

$$\hat{R} = \frac{\hat{Q}}{\hat{H}_0 - E_0}, \tag{8}$$

where E_0 is the ground-state energy given by the energy of the state depicted in Fig. 5. $\hat{H}_{\text{eff}}$ operates in the subspace S_0 formed by the degenerate ground states of $\hat{H}_0$, that is, the subspace of states produced by the direct product of atomic states like those in Fig. 5 in which the spins of the four electrons occupying the four d orbitals, from one Fe atom to the next, point either all up or all down. The operator $\hat{P}_0$ is a projection operator which projects into the subspace S_0 and $\hat{Q} = \hat{1} - \hat{P}_0$, that is, the operator which projects outside the subspace S_0. The above equation can be formally solved iteratively to yield the Rayleigh-Schrödinger expansion as a power series in $\hat{T}$. The leading term is $\hat{T}$ which, when restricted in this subspace S_0, becomes just the direct Fe-Fe hopping terms,

$$\hat{P}_0 \hat{T} \hat{P}_0 = - \sum_{\langle ij \rangle, \sigma, \nu\nu'} (t_{\nu\nu'} d^{(\nu')\dagger}_{j\sigma} d^{(\nu)}_{i\sigma} + \text{H.c.}). \tag{9}$$

On the right-hand side of the above equation we have omitted the projection operators by assuming that we will restrict ourselves to the subspace S_0.

In the following, in order to simplify the calculation, we will take $U^{(d)}_\nu = U$ to be independent of ν and we will assume that U is much larger than the atomic energy-level difference (which was found to be less than 1 eV within our TB approximation) and significantly larger than the hopping and hybridization parameters. In addition, we will take $U^{(d)}_{\nu \neq \nu'} = \bar{U}$, $U^{(sp)}_\nu = U_{sp}$, and $U^{(sp)}_{\alpha \neq \alpha'} = \bar{U}_{sp}$, i.e., to be independent of ν, ν' (or α, α').

IV. EFFECTIVE SPIN-SPIN INTERACTION HAMILTONIAN

A. Interaction between same-type Fe orbitals

First, there are the familiar second-order processes arising from the direct Fe-Fe hopping through the matrix elements $t_{\nu\nu}$ which give rise to an antiferromagnetic exchange interaction of the form

$$\mathcal{H}_{\nu,\nu} = J^{(2)}_{\nu,\nu} \sum_{\langle ij \rangle} \vec{S}^\nu_i \cdot \vec{S}^\nu_j, \tag{10}$$

TABLE IV. The second-order nn contribution to the spin-spin couplings is obtained from the matrix elements listed below (in units of eV^2) by multiplying them with $4/U$.

$t_{\nu\nu'}^2$	$d_{x^2-y^2}$	d_{xz}	d_{yz}	d_{xy}	d_{z^2}
$d_{x^2-y^2}$	0.048	0	0	0	0
d_{xz}	0	0.25	0.29	0	0
d_{yz}	0	0.29	0.25	0	0
d_{xy}	0	0	0	0.185	0.04
d_{z^2}	0	0	0	0.04	0.048

$$J_{\nu,\nu}^{(2)} = \frac{4t_{\nu,\nu}^2}{U}. \tag{11}$$

In addition, we have antiferromagnetic coupling of the spins of two different types of Fe d orbitals due to the hopping terms $t_{xz,yz}$ and t_{xy,z^2} which give rise to

$$\mathcal{H}_{\nu,\nu'} = J_{\nu,\nu'}^{(2)} \sum_{\langle ij \rangle} \vec{S}_i^{\nu} \cdot \vec{S}_j^{\nu'}, \tag{12}$$

$$J_{\nu,\nu'}^{(2)} = \frac{4t_{\nu,\nu'}^2}{U}, \tag{13}$$

where ν, ν' can be either xz, yz or xy, z^2. These processes take place only between nearest neighbors such as the Fe atoms 1 and 2 in Fig. 1. These second-order contributions are obtained from the square of the matrix elements listed in Table IV by multiplying them with $4/U$. There are no second-order next-nearest-neighbor (nnn) contributions to the spin-spin interaction.

The next terms to leading order, beyond the first- and second-order terms discussed above, are fourth-order processes involving an Fe d orbital and the As sp orbitals with which it hybridizes. The contribution of all sp orbitals of the two possible intervening As atoms to the exchange interaction between the same d orbital of two nn Fe atoms is given by[37]

$$\mathcal{H}_{\nu,\nu} = J_{\nu,\nu}^{(4)} \sum_{\langle ij \rangle} \vec{S}_i^{(\nu)} \cdot \vec{S}_j^{(\nu)}, \tag{14}$$

$$J_{\nu,\nu}^{(4)} = \sum_{\alpha=1}^{6} J_{\nu\nu}^{\alpha}, \tag{15}$$

$$J_{\nu\nu}^{\alpha} = 2b^2 \left[\frac{1}{U^*} + \frac{1}{U^* + \epsilon} \right], \quad b = \frac{V_1^{\alpha\nu} V_2^{\alpha\nu}}{U^* + \epsilon}, \tag{16}$$

where

$$U^* = U + 5\bar{U} - (4\bar{U}_{sp} + U_{sp}), \tag{17}$$

and U^* is assumed to be significantly larger than all other energy scales in the problem. Here

$$\epsilon = \epsilon_{sp}(\alpha) - \epsilon_d(\nu) \tag{18}$$

is the energy difference between the As sp state and that of the Fe d orbital. Subscripts 1 and 2 in the matrix elements

TABLE V. Fourth-order sum of matrix elements contributing to the nn spin-spin couplings.

$A_{\nu\nu'}$	$d_{x^2-y^2}$	d_{xz}	d_{yz}	d_{xy}	d_{z^2}
$d_{x^2-y^2}$	0.13	0.12	0.12	0.01	0.40
d_{xz}	0.12	0.04	0.24	0.08	0.40
d_{yz}	0.12	0.24	0.04	0.08	0.40
d_{xy}	0.01	0.08	0.08	0	0.01
d_{z^2}	0.40	0.40	0.40	0.01	1.31

refer to the fact that the two nn atoms 1 and 2 are at 90° angle relative to the position of the intervening As atom and, therefore, V_1 is from Table III, while V_2 is from Table III by interchanging indices 1 and 2 and the sign of the matrix elements.

Since $\epsilon < 1$ eV for any combination of Fe d and the three As sp orbitals and $U^* \sim 5$ eV, if ϵ is neglected in the above expression the error in our estimate for the exchange couplings J will be rather small. We are going to use the full expression given by Eq. (16) when we compute the coupling constants J between the same-type Fe orbitals. We will also use this approximation of neglecting ϵ because it simplifies the results and this gives additional insight. With this approximation, we find that

$$J_{\nu,\nu}^{(4)} \simeq \frac{4A_{\nu\nu}}{U^{*3}}, \tag{19}$$

$$A_{\nu\nu} = \sum_{\alpha=1}^{6} (V_1^{\alpha\nu} V_2^{\alpha\nu})^2. \tag{20}$$

Since the value of U^* is not known, we can use the expression given by Eq. (20) as a measure of the relative spin-exchange interaction coupling. Namely, to obtain the actual values of $J_{\nu\nu}^{(4)}$, and $J_{\nu\nu'}^{(4)}$ with $\nu \neq \nu'$ to be discussed next, we just need to multiply the values given in Table V by $4/(U^*)^3$. Therefore, for two nn Fe atoms, such as Fe atoms 1 and 2 in Fig. 1, the spin-spin interaction coupling constant $J_{\nu\nu}$ is obtained by adding the second- and fourth-order contributions $J_{\nu\nu}^{(2)}$ and $J_{\nu\nu}^{(4)}$, respectively.

On the other hand, for two nnn Fe atoms, such as 1 and 3 in Fig. 1, there are no second-order processes since there are no direct hopping between such atoms. The fourth-order superexchange contributions is obtained as follows:

$$\mathcal{H}_{\nu,\nu}' = J_{\nu,\nu}' \sum_{\langle\langle ij \rangle\rangle} \vec{S}_i^{(\nu)} \cdot \vec{S}_j^{(\nu)}, \tag{21}$$

$$J_{\nu,\nu}' = \frac{1}{2} \sum_{\alpha=1}^{6} J_{\nu\nu}'^{\alpha}, \tag{22}$$

$$J_{\nu\nu}'^{\alpha} = b'^2 \left[\frac{1}{U^*} + \frac{1}{U^* + \epsilon} \right], \quad b' = 2\frac{(V_1^{\alpha\nu})^2}{U^* + \epsilon}. \tag{23}$$

Notice that in this case the same matrix elements V_1 are involved because both atoms participating in the superex-

TABLE VI. Fourth-order sum of matrix elements contributing to the nnn spin-spin couplings.

$A'_{\nu\nu'}$	$d_{x^2-y^2}$	d_{xz}	d_{yz}	d_{xy}	d_{z^2}
$d_{x^2-y^2}$	0.18	0.46	0.46	0	0.42
d_{xz}	0.46	4.66	0	0	0.53
d_{yz}	0.46	0	4.66	0	0.53
d_{xy}	0	0	0	0	0
d_{z^2}	0.42	0.53	0.53	0	1.32

TABLE VII. Second-order terms contributing to the effective nn hopping.

$B_{\nu\nu'}$	$d_{x^2-y^2}$	d_{xz}	d_{yz}	d_{xy}	d_{z^2}
$d_{x^2-y^2}$	-0.50	0.31	0.31	0	0
d_{xz}	0.31	0.29	-0.49	-0.29	-0.65
d_{yz}	0.31	-0.49	0.29	0.29	0.65
d_{xy}	0	-0.29	0.29	0	0.1
d_{z^2}	0	-0.65	0.65	0.01	1.62

change form the same angle with the intervening As atoms. In addition, there is a factor of 2 difference between the above expression and Eq. (16) because there is only one possible intervening As atom for two fixed Fe atoms. The simplified expression, when ϵ is neglected, is the following:

$$J'^{(4)}_{\nu,\nu} \simeq \frac{4A'_{\nu\nu}}{U^{*3}}, \qquad (24)$$

$$A'_{\nu\nu} = \frac{1}{2}\sum_{\alpha=1}^{6}(V_1^{\alpha\nu})^4. \qquad (25)$$

The values of the constant $A'_{\nu\nu}$ are given as the diagonal matrix elements of Table VI.

B. Interaction between different-type Fe orbitals

There is an effective spin-spin interaction between certain Fe orbitals of different types, $J_{\nu\nu'}$ with $\nu \neq \nu'$. This type of nn and nnn spin-spin interactions for most of the orbitals is significantly smaller than the $J_{\nu\nu}$ coupling constants between the same orbitals. To obtain an estimate of these we use the simplified expressions where ϵ is neglected. Namely,

$$J^{(4)}_{\nu,\nu'} \simeq \frac{4A_{\nu\nu'}}{U^{*3}}, \qquad (26)$$

$$A_{\nu\nu'} = \sum_{\alpha=1}^{6}(V_1^{\alpha\nu}V_2^{\alpha\nu'})^2, \qquad (27)$$

$$J'^{(4)}_{\nu,\nu'} \simeq \frac{4A'_{\nu\nu'}}{U^{*3}}, \qquad (28)$$

$$A'_{\nu\nu'} = \frac{1}{2}\sum_{\alpha=1}^{6}(V_1^{\alpha\nu}V_1^{\alpha\nu'})^2. \qquad (29)$$

The values of the constants $A_{\nu\nu'}$ and $A'_{\nu\nu'}$ are given as the off-diagonal matrix elements of Tables V and VI.

C. Hopping between same-type Fe orbitals

There are contributions to the effective hopping matrix elements due to second-order processes. Namely, processes in which an electron from a doubly occupied As orbital momentarily hops to the nn Fe d orbital and then an electron

from the doubly occupied doped d orbital hops to the singly occupied As orbital left behind. These processes give rise to the following expression:

$$\delta t_{\nu,\nu} = \sum_{\alpha=1}^{6} \frac{V_1^{\alpha\nu}V_2^{\alpha\nu}}{U^* + \epsilon}, \qquad (30)$$

where ϵ is given by Eq. (18). Again, since the value of U^* is not known, for large enough values of U^* ($\epsilon < 1$ eV) we can neglect ϵ in the above expression to obtain the following expression:

$$\delta t_{\nu,\nu} = \frac{B_{\nu\nu}}{U^*}, \qquad (31)$$

$$B_{\nu\nu} = \sum_{\alpha=1}^{6} V_1^{\alpha\nu}V_2^{\alpha\nu}, \qquad (32)$$

and the values of $B_{\nu\nu}$ are given as the diagonal elements in Table VII. The actual estimates for $\delta t_{\nu\nu}$ can be obtained by dividing the values in the table by U^*. The total effective nn hopping is given as

$$\tilde{t}_{\nu\nu} = t_{\nu\nu} + \delta t_{\nu\nu}. \qquad (33)$$

In the case of nnn such as the Fe atoms 1 and 3 in Fig. 1 we obtain

$$\tilde{t}'_{\nu\nu} = \frac{B'_{\nu\nu}}{U^*}, \qquad (34)$$

$$B'_{\nu\nu} = \frac{1}{2}\sum_{\alpha=1}^{6}(V_1^{\alpha\nu})^2. \qquad (35)$$

The values of $B'_{\nu\nu}$ are given as the diagonal elements of Table VIII.

D. Hopping between different-type Fe orbitals

There is a second-order process by means of which a doubly occupied site can effectively hop to a nn Fe d orbital of different types by involving an intervening As sp orbital. These contributions are smaller than those connecting two of the same-type Fe d orbitals and they can be approximated by

$$\delta t_{\nu,\nu'} = \frac{B_{\nu\nu'}}{U^*}, \qquad (36)$$

TABLE VIII. Second-order terms contributing to the effective nnn hopping.

$B'_{\nu\nu'}$	$d_{x^2-y^2}$	d_{xz}	d_{yz}	d_{xy}	d_{z^2}
$d_{x^2-y^2}$	0.82	−0.93	−0.93	0	0
d_{xz}	−0.93	2.60	0	−0.02	−0.99
d_{yz}	−0.93	0	2.60	0.02	0.99
d_{xy}	0	−0.02	0.02	0.08	0
d_{z^2}	0	−0.99	0.99	0	1.74

$$B_{\nu\nu'} = \sum_{\alpha=1}^{6} V_1^{\alpha\nu} V_2^{\alpha\nu'}. \tag{37}$$

The values of $B_{\nu\nu'}$ are given by the off-diagonal elements of Table VII.

There is also a second-order process which gives rise to hopping between nnn Fe d orbitals of different types. For this case we obtain

$$\delta t'_{\nu,\nu'} = \frac{B'_{\nu\nu'}}{U^*}, \tag{38}$$

$$B'_{\nu\nu'} = \sum_{\alpha=1}^{6} V_1^{\alpha\nu} V_1^{\alpha\nu'}. \tag{39}$$

The values of $B'_{\nu\nu'}$ are given by the off-diagonal elements of Table VIII.

The total effective nn and nnn hoppings for $\nu \neq \nu'$ are given as

$$\tilde{t}_{\nu\nu'} = t_{\nu\nu'} + \delta t_{\nu\nu'}, \tag{40}$$

$$\tilde{t}'_{\nu\nu'} = \delta t'_{\nu\nu'}. \tag{41}$$

E. Effective Hamiltonian

In summary the effective Hamiltonian is given by

$$\mathcal{H}_{\text{eff}} = \sum_{\nu,\nu'} \mathcal{H}_{\nu\nu'} - J^H \sum_{i,\mu,\mu'} \vec{S}_i^\mu \cdot \vec{S}_i^{\mu'}, \tag{42}$$

where each of the $\mathcal{H}_{\nu,\nu'}$ terms above may be written as

$$\mathcal{H}_{\nu,\nu'} = -\sum_{\langle ij\rangle,\sigma} \tilde{t}_{\nu,\nu'} c_{j\nu'\sigma}^\dagger c_{i\nu\sigma} - \sum_{\langle\langle ij\rangle\rangle,\sigma} \tilde{t}'_{\nu,\nu'} c_{j\nu'\sigma}^\dagger c_{i\nu\sigma}$$
$$+ \sum_{\langle ij\rangle} J_{\nu,\nu'} \vec{S}_i^\nu \cdot \vec{S}_j^{\nu'} + \sum_{\langle\langle ij\rangle\rangle} J'_{\nu,\nu'} \vec{S}_i^\nu \cdot \vec{S}_j^{\nu'}. \tag{43}$$

Next, we will provide estimates of the coupling constants $\tilde{t}_{\nu,\nu'}$, $\tilde{t}'_{\nu,\nu'}$, $J_{\nu,\nu'}$, and $J'_{\nu,\nu'}$ involved in the above model based on the values of the parameters obtained from fitting the LDA results to the tight-binding model. The matrix elements for nn hopping $\tilde{t}_{\nu\nu'}$ and spin-spin interaction $J_{\nu\nu'}$ as well as their counterparts for nnn interactions—that is, between sites diagonally across in the square lattice formed by the Fe atoms, $\tilde{t}'_{\nu\nu'}$ and $J'_{\nu\nu'}$—are given in Tables IX and X for $U^*=U=5$ eV and in Tables XI and XII for $U_\nu^*=U=3$ eV. A more simplified model than the one given above is discussed in Sec. V.

V. DISCUSSION

First, by examining Tables IX–XII, we notice that to a reasonable degree of approximation the following three subspaces couple with each other rather weakly: (a) one spanned by the $d_{x^2-y^2}$ Fe orbital, (b) one spanned by the degenerate atomic Fe orbitals d_{xz} and d_{yz}, and (c) one spanned by the atomic Fe orbitals d_{xy} and d_{z^2}. Notice that the most significant off-diagonal matrix elements are those which couple d_{xz} to the d_{yz} orbital and those which couple d_{xy} to the d_{z^2} orbital. There are other smaller off-diagonal matrix elements which couple these subspaces weakly. These three subspaces, however, are much more strongly coupled through J^H.

We consider the undoped (LaOFeAs) case first. Because six electrons should occupy the five Fe d orbitals (see Fig. 5), the lowest-energy subspace spanned by $d_{x^2-y^2}$ is occupied by two electrons, and also each of the other two subspaces is also occupied by two electrons. As mentioned above, these three subspaces are coupled mainly because $J^H \neq 0$. Furthermore, the bands formed in any given subspace are intersected

TABLE IX. The estimated matrix elements for $J_{\nu\nu'}$ and $J'_{\nu\nu'}$ for $U=5$ eV.

J, J'	$d_{x^2-y^2}$	d_{xz}	d_{yz}	d_{xy}	d_{z^2}
$d_{x^2-y^2}$	0.04	0.0	0.0	0.0	0.01
	0	0	0.01	0.01	0.01
d_{xz}	0.0	0.20	0.24	0.0	0.01
	0.01	0.07	0	0.0	0.01
d_{yz}	0.0	0.24	0.20	0.0	0.01
	0.01	0	0.07	0.0	0.01
d_{xy}	0.0	0.0	0.0	0.15	0.03
	0	0	0	0	0
d_{z^2}	0.01	0.01	0.01	0.03	0.08
	0.01	0.01	0.01	0.0	0.02

TABLE X. The estimated matrix elements for $t_{\nu\nu'}$ and $t'_{\nu\nu'}$ for $U=5$ eV.

$\tilde{t}, \tilde{t}'$	$d_{x^2-y^2}$	d_{xz}	d_{yz}	d_{xy}	d_{z^2}
$d_{x^2-y^2}$	0.12	0.06	0.06	0	0
	0.08	−0.09	−0.09	0	0
d_{xz}	0.06	0.56	0.44	−0.06	−0.13
	−0.09	0.26	0	0	−0.1
d_{yz}	0.06	0.44	0.56	0.06	0.13
	−0.09	0	0.26	0	0.1
d_{xy}	0	−0.06	0.06	0.43	0.22
	0	0	0	0.01	0
d_{z^2}	0	−0.13	0.13	0.22	0.54
	0	−0.1	−0.1	0	0.17

TABLE XI. The estimated matrix elements for $J_{\nu\nu'}$ and $J'_{\nu\nu'}$ for $U = 3$ eV.

J, J'	$d_{x^2-y^2}$	d_{xz}	d_{yz}	d_{xy}	d_{z^2}
$d_{x^2-y^2}$	0.08	0.02	0.02	0	0.06
	0.01	0.03	0.03	0	0.03
d_{xz}	0.02	0.34	0.42	0.01	0.06
	0.03	0.35	0	0	0.04
d_{yz}	0.02	0.42	0.34	0.01	0.06
	0.03	0	0.35	0	0.04
d_{xy}	0	0.01	0.01	0.25	0.05
	0	0	0	0	0
d_{z^2}	0.06	0.06	0.06	0.05	0.26
	0.03	0.04	0.04	0	0.10

TABLE XII. The estimated matrix elements for $t_{\nu\nu'}$ and $t'_{\nu\nu'}$ for $U = 3$ eV.

$\tilde{t}, \tilde{t}'$	$d_{x^2-y^2}$	d_{xz}	d_{yz}	d_{xy}	d_{z^2}
$d_{x^2-y^2}$	0.05	0.10	0.10	0	0
	0.14	−0.16	−0.16	0	0
d_{xz}	0.10	0.60	0.38	−0.10	−0.22
	−0.16	0.43	0	0	−0.17
d_{yz}	0.10	0.38	0.60	0.10	0.22
	−0.16	0	0.43	0	0.17
d_{xy}	0	−0.10	0.10	0.43	0.23
	0	0	0	0.01	0
d_{z^2}	0	−0.22	0.22	0.23	0.76
	0	−0.17	0.17	0	0.29

by the bands formed in the other two subspaces because their atomic energy difference is small compared to their bandwidth.

There is a great degree of magnetic frustration, as noted in Refs. [20], [21], and [25], especially in the subspace spanned by d_{xz}/d_{yz}. In this subspace the nnn coupling J' becomes greater than $J/2$ for any value of $U^* \le 4.3$ eV (see Fig. [6]). When $J < 2J'$, the observed columnar antiferromagnetic ordering is favorable[21],[25] relative to the familiar (π, π) antiferromagnetic order. The subspace spanned by $d_{x^2-y^2}$ has net spin zero and, therefore, is not expected to contribute significantly to the choice of magnetic order. On the other hand, there seems to be less frustration in the subspace spanned by d_{xy}/d_{z^2}, which is half-filled; we therefore expect that a long-range antiferromagnetic order should characterize the ground state of this subspace if it were uncoupled from the d_{xz}/d_{yz} subspace. However, due to Hund's rule coupling J^H, the spin orientation of all subspaces should be common. The conflicting preferences of these two subspaces, which are forced to make a common choice, introduce further frustration of relative spin orientation.
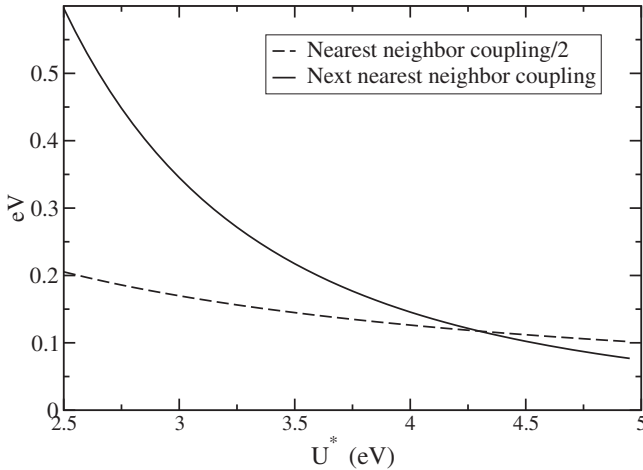

FIG. 6. The calculated nn $J_{xz,xz}/2$ is compared to the nnn $J'_{xz,xz}$ as a function of $U^* = U$. The condition for the instability of the (π, π) order to the columnar order is $J'_{xz,xz} > J_{xz,xz}/2$ which occurs for values of $U^* \le 4.3$ eV.

We expect that the subspace spanned by d_{xz}/d_{yz} drives the system to a global columnar order[20],[21],[25] because it is characterized by the larger couplings. The presence of a large J' in the subspace spanned by d_{xz}/d_{yz} might impose the $(0, \pi)$ order through the relatively large Hund's rule coupling $J_H \sim 0.5$ eV. The fact that the subspace d_{xz}/d_{yz} prefers the columnar order and the subspace d_{z^2}/d_{xy} prefers the (π, π) order creates frustration which may also explain the fact that the observed moment per Fe atom is small.

We emphasize that unlike the case of undoped cuprates, the undoped parent compound in the case of the oxypnictides is not an insulator. As can be inferred from Fig. [1], the motion along the ferromagnetic direction is not hindered and, therefore, the undoped material is expected to demonstrate anisotropic transport in the SDW phase.

We would like to discuss the case of the neutral FeAs layer which was considered in Sec. II, where it was found that the ground state is characterized by (π, π) order. The case of the neutral layer has five electrons per Fe atom and this implies that all Fe d orbitals should be singly occupied. Therefore, the subspace spanned by $d_{x^2-y^2}$ is no longer characterized by spin zero. This means that the subspace d_{xz}/d_{yz} in order to drive the columnar order has to compete against not just one but two subspaces which prefer the (π, π) order.

The phenomenological Hamiltonian considered in Ref. [20], [21], and [25] to introduce frustration is different from the one we derived based on a more rigorous approach, which is more complex. The next step would be to study the Hamiltonian given in Eqs. ([42]) and ([43]) by various analytical and numerical techniques, which is beyond the scope of the present work.

While the estimated nn antiferromagnetic coupling constants are of similar magnitude to the one in the cuprous oxides,[38] in the oxypnictide materials there is magnetic frustration mainly due to the fact that the nnn antiferromagnetic coupling for the d_{xz}/d_{yz} subspace is large. Therefore, assuming that the pairing interaction between electrons is of magnetic origin, it is not clear if the pairing energy scale is larger or smaller compared to that in the cuprate superconducting materials. The pairing energy scale in the present model may be enhanced by the "flavor" factor, that is, the number of states spanning the subspace where the added electrons go in

the case of electron doping, and by the fact that the hopping and spin-exchange matrix elements are estimated to be somewhat larger compared to those in the case of the cuprates (see Tables IX–XII). Therefore, it is conceivable that this new class of superconductors could lead to higher critical temperatures upon future optimization of the doping agents and other factors.

A very important difference between the oxypnictides and the cuprates is that the fivefold sector can be thought of as formed by three subsectors, two two-flavor sectors and one one-flavor sector. The d_{xz}/d_{yz} sector prefers the SDW order depicted in Fig. 1; the sector spanned by the $d_{x^2-y^2}$ orbital has spin zero and the other sector spanned by d_{xy}/d_{z^2} prefers antiferromagnetic long-range order. These subspaces are coupled by Hund's rule which, we believe, leads to the SDW order with ferromagnetic order along one direction and antiferromagnetic ordering between such chains. As in the case of cuprates, superconductivity in the oxypnictide materials might coexist with SDW order[39] but these are expected to be to some extent competing orders as found in neutron[40] and μSR studies[41] done on the superconducting doped materials.

[1] Y. Kamihara, H. Hiramatsu, M. Hirano, R. Kawamura, H. Yanagi, T. Kamiya, and H. Hosono, J. Am. Chem. Soc. **128**, 10012 (2006).

[2] Y. Kamihara, T. Watanabe, M. Hirano, and H. Hosono, J. Am. Chem. Soc. **130**, 3296 (2008).

[3] Z.-A. Ren, J. Yang, W. Lu, W. Yi, G.-C. Che, X.-L. Dong, L.-L. Sun, and Zhong-Xian Zhao, Mater. Res. Innovations **12**, 105 (2008); Z.-A. Ren, W. Lu, J. Yang, W. Yi, X.-L. Shen, Z.-C. Li, G.-C. Che, X.-L. Dong, L.-L. Sun, F. Zhou, and Z.-X. Zhao, Chin. Phys. Lett. **25**, 2215 (2008).

[4] X. H. Chen, T. Wu, G. Wu, R. H. Liu, H. Chen, and D. F. Fang, Nature (London) **453**, 761 (2008).

[5] G. F. Chen, Z. Li, D. Wu, G. Li, W. Z. Hu, J. Dong, P. Zheng, J. L. Luo, and N. L. Wang, Phys. Rev. Lett. **100**, 247002 (2008).

[6] Hai-Hu Wen, Gang Mu, Lei Fang, Huan Yang, and Xiyu Zhu, Europhys. Lett. **82**, 17009 (2008).

[7] D. J. Singh and M.-H. Du, Phys. Rev. Lett. **100**, 237003 (2008).

[8] I. I. Mazin, D. J. Singh, M. D. Johannes, and M. H. Du, Phys. Rev. Lett. **101**, 057003 (2008).

[9] K. Haule, J. H. Shim, and G. Kotliar, Phys. Rev. Lett. **100**, 226402 (2008).

[10] L. Boeri, O. V. Dolgov, and A. A. Golubov, Phys. Rev. Lett. **101**, 026403 (2008).

[11] C. Cao, P. J. Hirschfeld, and H. P. Cheng, Phys. Rev. B **77**, 220506(R) (2008).

[12] A. O. Shorikov, M. A. Korotin, S. V. Streltsov, S. L. Skornyakov, D. M. Korotin, and V. I. Anisimov, arXiv:0804.3283 (unpublished).

[13] Q. Si and E. Abrahams, Phys. Rev. Lett. **101**, 076401 (2008).

[14] E. Z. Kurmaev, R. G. Wilks, A. Moewes, N. A. Skorikov, Yu. A. Izyumov, L. D. Finkelstein, R. H. Li, and X. H. Chen, arXiv:0805.0668 (unpublished).

[15] T. Miyake and F. Aryasetiawan, Phys. Rev. B **77**, 085122 (2008).

[16] B.-L. Yu, J. C. F. Wang, A. D. Beyer, M. L. Teague, J. S. A. Horng, S.-P. Lee, and N.-C. Yeh, arXiv:0804.4028 (unpublished).

[17] K. Kuroki, S. Onari, R. Arita, H. Usui, Y. Tanaka, H. Kontani, and H. Aoki, Phys. Rev. Lett. **101**, 087004 (2008).

[18] Zi-Jian Yao, Jian-Xin Li, and Z. D. Wang, arXiv:0804.4166 (unpublished).

[19] Xiao-Liang Qi, S. Raghu, Chao-Xing Liu, D. J. Scalapino, and Shou-Cheng Zhang, arXiv:0804.4332 (unpublished).

[20] T. Yildirim, Phys. Rev. Lett. **101**, 057010 (2008).

[21] Fengjie Ma, Zhong-Yi Lu, and Tao Xiang, arXiv:0804.3370 (unpublished).

[22] S. Raghu, X. L. Qi, C. X. Liu, D. J. Scalapino, and S. C. Zhang, Phys. Rev. B **77**, 220503(R) (2008).

[23] P. A. Lee and X.-G. Wen, Phys. Rev. B **78**, 144517 (2008).

[24] V. Cvetkovic and Z. Tesanovic, arXiv:0804.4678 (unpublished).

[25] C. Xu, M. Müller, and S. Sachdev, Phys. Rev. B **78**, 020501(R) (2008).

[26] Z.-Y. Weng, arXiv:0804.3228 (unpublished).

[27] J. Li and Y. Wang, Chin. Phys. Lett. **25**, 2232 (2008).

[28] K. Haule and G. Kotliar, arXiv:0805.0722 (unpublished).

[29] J. Dong, H. J. Zhang, G. Xu, Z. Li, G. Li, W. Z. Hu, D. Wu, G. F. Chen, X. Dai, J. L. Luo, Z. Fang, and N. L. Wang, Europhys. Lett. **83**, 27006 (2008).

[30] Clarina de la Cruz, Q. Huang, J. W. Lynn, Jiying Li, W. Ratcliff II, J. L. Zarestky, H. A. Mook, G. F. Chen, J. L. Luo, N. L. Wang, and Pengcheng Dai, Nature (London) **453**, 899 (2008).

[31] H. H. Klauss, H. Luetkens, R. Klingeler, C. Hess, F. J. Litterst, M. Kraken, M. M. Korshunov, I. Eremin, S. L. Drechsler, R. Khasanov, A. Amato, J. Hamann-Borrero, N. Leps, A. Kondrat, G. Behr, J. Werner, and B. Buchner, Phys. Rev. Lett. **101**, 077005 (2008).

[32] J. M. Soler, E. Artacho, J. D. Gale, A. García, J. Junquera, P. Ordejón, and D. Sánchez-Portal, J. Phys.: Condens. Matter **14**, 2745 (2002).

[33] N. Troullier and J. L. Martins, Phys. Rev. B **43**, 1993 (1991).

[34] D. M. Ceperley and B. J. Alder, Phys. Rev. Lett. **45**, 566 (1980).

[35] G. Kresse and J. Furthmuller, Phys. Rev. B **54**, 11169 (1996).

[36] P. E. Blöchl, Phys. Rev. B **50**, 17953 (1994).

[37] J. H. Jefferson, J. Phys. C **21**, L193 (1988).

[38] E. Manousakis, Rev. Mod. Phys. **63**, 1 (1991).

[39] A. J. Drew, F. L. Pratt, T. Lancaster, S. J. Blundell, P. J. Baker, R. H. Liu, G. Wu, X. H. Chen, I. Watanabe, V. K. Malik, A. Dubroka, K. W. Kim, M. Roessle, and C. Bernhard, Phys. Rev. Lett. **101**, 097010 (2008).

[40] Y. Qiu, M. Kofu, Wei Bao, S.-H. Lee, Q. Huang, T. Yildirim, J. R. D. Copley, J. W. Lynn, T. Wu, G. Wu, and X. H. Chen, Phys. Rev. B **78**, 052508 (2008).

[41] J. P. Carlo, Y. J. Uemura, T. Goko, G. J. MacDougall, J. A. Rodriguez, W. Yu, G. M. Luke, Pengcheng Dai, N. Shannon, S. Miyasaka, S. Suzuki, S. Tajima, G. F. Chen, W. Z. Hu, J. L. Luo, and N. L. Wang, arXiv:0805.2186 (unpublished).